Journal of Environmental Radioactivity 219 (2020) 106273

Contents lists available at ScienceDirect

Journal of Environmental Radioactivity

journal homepage: http://www.elsevier.com/locate/jenvrad

Micro-analytical characterization of thorium-rich aggregates from Norwegian NORM sites (Fen Complex, Telemark)

Simone Cagno [a,*], Ole Christian Lind [a], Jelena Mrdakovic Popic [a,b], Lindis Skipperud [a], Wout De Nolf [c], Gert Nuyts [d], Frederik Vanmeert [d], Jakub Jaroszewicz [e], Koen Janssens [d], Brit Salbu [a]

[a] Norwegian University of Life Sciences, Center of Excellence in Environmental Radioactivity (CERAD), Faculty of Environmental Sciences and Natural Resource Management, P.O. Box 5003, 1433 Ås, Norway
[b] Norwegian Radiation and Nuclear Safety Authority (DSA), PO Box 329 Skøyen, 0213, Oslo, Norway
[c] European Synchrotron Radiation Facility, Avenue des Martyrs 71, 38043, Grenoble Cedex 9, France
[d] AXES, University of Antwerp, Groenenborgerlaan 121, 2020, Antwerpen, Belgium
[e] Faculty of Materials Science, Warsaw University of Technology, Woloska 141, 02-507, Warsaw, Poland

ARTICLE INFO

Keywords:
Thorium
NORM
REE
Radioactive particles
Electron microscopy
Synchrotron radiation
μ-XRF
μ-XRD
μ-CT

ABSTRACT

In this study we performed microscopic characterization of mineral particles that were collected in the thorium-rich Fen Complex in Norway and identified and isolated based on autoradiography in function of their radioactivity. For this we combined information obtained with X-ray absorption μ-CT, μ-XRF and μ-XRD, both in bi- and in three-dimensional (tomographic) mode. We demonstrate that radionuclides and metals are heterogeneously distributed both within soil samples and within individual Th-enriched aggregates, which are characterised as low-density mineral bulk particles with high density material inclusions, where Th as well as several metals are highly concentrated. For these sites, it is important to take into account how these inhomogeneous distributions could affect the overall environmental behaviour of Th and progeny upon weathering due to human or environmental factors. Moreover, the estimated size of the Th-containing inclusions as determined in this work represents information of importance for the characterization of radionuclides and toxic metals exposure, as well as for assessing the viability of mining for Th and rare-earth metals in the Fen Complex and the associated environmental impact.

1. Introduction

Most Naturally Occurring Radioactive Materials (NORM) exist in rocks, soil and sediments in levels that are neither of particular radiological concern to human or environmental health, nor of potential industrial value. However, in certain geologically specific areas worldwide, bedrocks are enriched in the primordial radionuclides of uranium (^{238}U) and thorium (^{232}Th), often accompanied with rare earth elements (REE) and heavy metals. Changes in environmental conditions (naturally or due to human activities) can potentially result in increased weathering, mobilization of NORM and consequently their bioavailability for uptake in biota and/or entering the food chain. Thus, the most common steps prior to possible mining activities in such areas are: (a) the assessment of potential environmental risks including radiological aspects and (b) the evaluation of economic viability and potential for mining.

The Fen Complex is situated in the Telemark county, southern Norway and comprises former iron (Fe) and niobium (Nb) mines, namely the Fen and the Søve mining sites, respectively. This area is known for its significant levels of Th-bearing minerals and high levels of other metals including U and arsenic (As) (Killeen and Heier, 1976; Stranden, 1984, 1985).

Recently, the large Th and REE ore deposits located in this area have received a lot of attention. In particular, studies were conducted to assess (a) the environmental issues linked to undisturbed ^{232}Th rich and NORM legacy sites in the area, and (b) economic value and possibilities for future use of present ore deposits. These two aspects will be further described hereafter. Macroscopic and microscopic (i.e., with μm detail) chemical, mineral and grain-size information would be beneficial for both (a) and (b), but such characterization of soil and rocks from the Fen

* Corresponding author.
E-mail address: simone.cagno@nmbu.no (S. Cagno).

https://doi.org/10.1016/j.jenvrad.2020.106273
Received 23 December 2019; Received in revised form 5 April 2020; Accepted 12 April 2020
Available online 27 April 2020

Complex has so far been scarce. In this paper we present the first application of a set of advanced micro-analytical techniques on relevant samples from several sites in the Fen Complex.

1.1. Assessment of potential environmental risks

The external gamma dose rates in the Fen Complex are among the highest in Europe reaching up to maximal 10 μGy/h (Dahlgren, 1983, Mrdakovic Popic et al., 2011), being the major contributor to the exposure dose to the population. While the worldwide median concentration of Th in soil is estimated in 7–8 mg/kg, the measured concentrations of ^{232}Th in rødberg rocks and soils collected at locations within or near the Fen Fe-mine range broadly between 97 and 3000 mg/kg (Sundal and Strand, 2004; Dahlgren, 1983, Mrdakovic Popic et al., 2011). Extensive mining has been conducted in the past, and remaining waste and soil in the area contain significant amounts of Th and U, as well as several stable metals. A wide range of ^{232}Th activity concentrations and very heterogeneous radionuclide distributions have been reported for Fen Complex soils, indicating the presence of radioactive particles (Mrdakovic Popic et al., 2011, 2012). Sequential extraction data showed ^{232}Th and progenies to be largely associated with (up to 95%) the residual soil fraction (Mrdakovic Popic et al., 2011, 2012), lending support to the view that radioactive particles carry a major fraction of the NORM radionuclides at these sites. Thus, particle characteristics such as composition, particle size and crystalline structures will influence weathering rates and subsequent mobilization, as well as radon emanation (Haquin et al., 2017).

Considering the abundance of NORM both undisturbed and altered by human activities in the past, the presence of several other stable metals, which can act as multiple stressors, and the potential for future mining activities, the Fen Complex is an appropriate natural laboratory for assessing the risks of NORM particles. Knowledge of the radionuclide distribution in the soil and the associated levels of other metals is desired in order to accurately assess radiological risks and to implement adequate radioprotection measures, when needed.

1.2. Possible economic value and use of thorium and associated REE

A future thorium nuclear fuel cycle would have some potential advantages over the current uranium fuel cycle; due to short half-life of ^{220}Rn the dose exposure during mining of Th (front end) is lower compared to U, and the waste products (back end) are less radioactive (no Pu produced) in the ^{232}Th/^{233}U cycle compared to the U/Pu cycle (Thorium Report Committee, 2008). In addition, Th is a more abundant resource than U. Especially in countries with monazite deposits such as India, Th based reactors are being further developed. For these factors, there is a renewed interest in the feasibility of the exploitation of known Th-deposits (IAEA, 2010).

In the Fen Complex, the size of the mineral grains in which Th is contained and the amount of Th are the main unknown factors for the determination of the Th extraction potential. Moreover, the economic benefit of Th mining would have to counterbalance possible licensing issues and radioactive waste disposal costs. The same goes for potential mining of co-occurring REE in the area, which would have to be separated from thorium, generating Th-tailings as well. Such Th-tailings disposal issues have hampered monazite processing elsewhere (Hoatson, 2011). Therefore, a more detailed characterization of the deposits of Th and associated elements in rocks and soils of this area can help to quantify the potential economic value of the Th-deposits, and indirectly of the REE deposits.

2. Materials and methods

2.1. Sites

Two legacy NORM sites (Fen and Søve) and one undisturbed Th-rich site (Bolladalen) were the object of this investigation.

The Fen site is a former mining area. It comprises a former Fe-mine in the location called Gruveåsen, and surrounding areas. The site consists of rødbergite type rock, rich in Fe and Th. Iron mining took place here between 1652 and 1926. Ore exploitation was conducted in open pits and underground tunnels; data on the exact mined quantities over the course of time are not available (Stranden, 1982; Dahlgren, 2005; NGI-UMB, 2010). The largest Th resources are estimated to be in the Gruveåsen location, where also the highest terrestrial gamma doses are registered (Dahlgren, 2012).

The Søve site is also a former mining area. It comprises a decommissioned niobium (Nb) facility in the western part of the Fen Complex and is characterised predominantly by the søvite rock type. Mining activity targeted this particular rock, consisting mainly of calcium carbonate ($CaCO_3$) (75–95%) and accessory minerals rich in Nb and to a lesser extent Th and U, such as pyrochlore [$(Na,Ca)_2Nb_2O_6(OH,F)$], columbite (Nb_2O_6) and fersmite [$(Ca,Ce,Na)(Nb,Ta,Ti)_2(O,OH,F)_6$] (Dahlgren, 2005). Fe-Nb production occurred on a commercial basis from 1953 to 1965. About 1.15 million tons søvite were extracted in total and went through extraction processes including crushing, separation and centrifugation, followed by thermal treatment. Lack of proper liquid and solid waste management, by today's standards, resulted in releases of actinides into the environment via discharges into the water stream, or production of slag and crushed residues, left on site. As a remediation measure, the affected areas were partly covered with sand and nowadays the site is freely accessible (Dahlgren, 1983, 2005).

The Bolladalen site is part of the large wooded area in the centre of the Fen Complex. Rødbergite is the main type of rock. The investigated sites are located in undisturbed wooded environment, with the exception of a few walking paths. Significantly enhanced NORM has been measured at this site earlier, both as elevated terrestrial gamma dose rates and rock and soil NORM activity concentrations (Mrdakovic Popic et al., 2011).

2.2. Macroscopic screening

Soil and rock samples were collected at the sites described above during fieldworks in 2009–2011. The accurate geographical positions of the sampling and measurement points were recorded using the Global Positioning System (GPS). The soil sampling methods used followed guidelines for environmental sampling for radionuclide analysis in the Nordic countries (Taipale, 1985) as well as international standard (US EPA, 2014). Sampling sites were approximately 100 m × 100 m (1 ha); bulk samples of surface and subsurface soil were taken in the O and A horizons (at depth 0–25 cm) by spoons, and at certain points by a custom designed soil corer. At each site, five soil sub-samples were pooled to an approximate fresh weight of 500 g, homogenized and considered to be representative. The abundance of background rocks in soil layers was a limitation and a challenge for deeper soil sampling in the whole area. Rock samples were randomly taken at investigated sites; at least ten separate rock samples were taken at each of the sites. Rock types were identified in the laboratory. After collection, soil samples were dried according to ISO standard 11464:2006E and homogenized by passing through a 2-mm mesh sieve, while rock samples were milled and stored until analysis.

Autoradiography was used to screen environmental samples for heterogeneities of radioactivity (Salbu and Lind, 2020) by using digital phosphor imaging (image plate and image plate scanner, Typhoon 8600, Molecular Dynamics). Subsamples constituted by particles and rock fragments were selected for further analysis based on their enhanced radioactivity as determined by digital autoradiography and were mechanically separated from the remainder of the samples.

2.3. Microscopic screening

The sub-samples localised and selected by means of digital

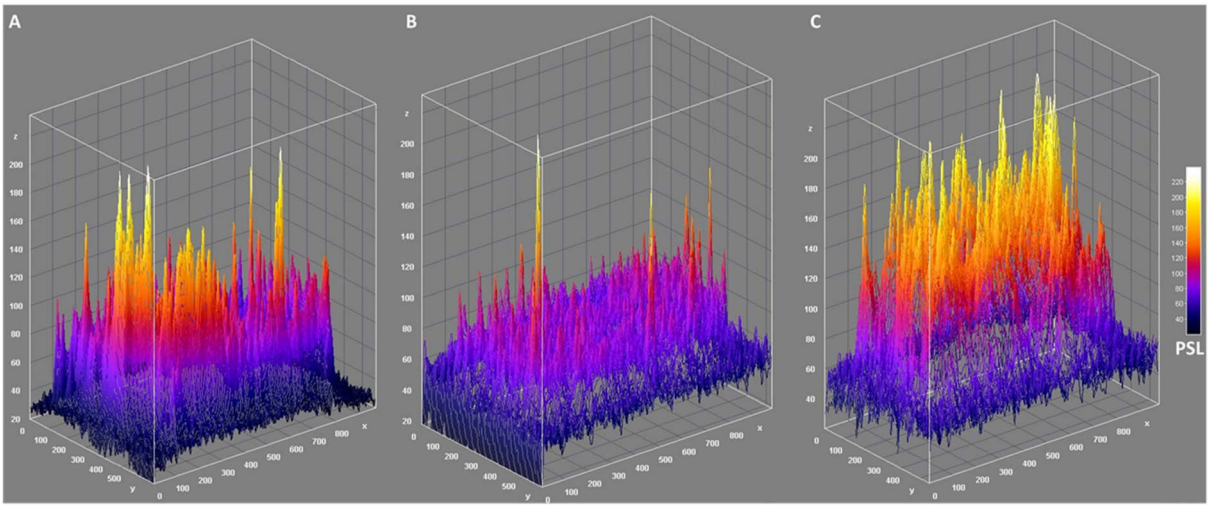

Fig. 1. Digital autoradiography of soils collected from the a) Fen, b) Søve and c) Bolladalen sites reflects inhomogeneous distributions of radioactivity. Read-out signals from the exposed image plates are reported as PhotoStimulable Luminescence (PSL).

autoradiography were characterised using a Zeiss EVO 50 variable pressure Environmental Scanning Electron Microscope (ESEM) interfaced with Energy Dispersive X-ray analysis (EDX). ESEM-EDX allowed a first elemental characterization. However, this is typically hampered by the limit of detection (0.1% w/w for 100 s live time).

Therefore, sub-samples were selected for more sensitive microanalytical X-ray techniques. In some cases, sub-sub-samples constituted by single particles were separated mechanically by the rest of the samples with the help of surgical blades and tweezers under an optical microscope, in light of the information retrieved with the previous techniques. The 3D morphology was explored by X-ray absorption microtomography (μ-CT), while elemental and mineralogical information were obtained by synchrotron-based micro-X-ray fluorescence and micro-X-ray-diffraction, respectively.

2.4. Micro-tomography

At the Faculty of Materials Science and Engineering of the Warsaw University of Technology, a laboratory μ-CT scanner was used to image the soil particles, which were glued on glass capillaries. The instrument used was an XRadia MicroXCT-400, equipped with a Hamamatsu 150 kV X-ray source and a 2 K Andor CCD camera. In addition to the geometric magnification, it also includes a set of scintillator-coated objective lenses with an optical magnification of 0.5X, 4X, 10X, 20X and 40X, that allow sub-μm resolution. Reconstructions were performed using an algorithm based on cone-beam filtered back-projection, including ring artefact and beam hardening corrections (Kak and Slaney, 1988). The latter is required since a polychromatic primary beam is used.

CT imaging allowed 3D reconstruction of whole particles with a 1 μm resolution. The output consists of a stack of tomograms (virtual slices) that show the inner morphology of the samples in grey tones, which represent the X-ray attenuation at each location. By using commercial software (VG Studio Max, Skyscan Dataviewer) it is possible to navigate through the sample in all three dimensions and to analyse the image stack. Through segmentation, it is possible to isolate only the desired phases/volume portions, in function of their X-ray attenuation. The relative abundances of the different phases can then be calculated as volume percentages.

2.5. Synchrotron experiments

Selected particles and rock fragments, mounted on flat sample holders using carbon tape or glued on glass capillaries, were analysed with combined micro-X-ray fluorescence (μ-XRF) and micro-X-ray powder diffraction (μ-XRD), in scanning (2D) and tomographic (3D) modes, performed at beamline L, HASYLAB synchrotron, Hamburg, Germany.

A focused monochromatic X-ray microbeam of 10–15 μm diameter (primary energy 20.2 keV), having a divergence of ~4 mrad was used for the investigations. This beam was obtained by employing a 200 period Mo/Si multilayer monochromator with mean layer thickness of 2.98 nm for energy band selection ($\Delta E/E = 1\%$) and a single-bounce elliptical capillary for beam focussing (Falkenberg et al., 2004). A 1 K Bruker CCD camera positioned behind the sample was used for collecting diffraction patterns in transmission mode, along with two silicon drift detectors (SDD), positioned at 90 and 270° relative to the primary X-ray beam, for simultaneous detection of the XRF signals.

Confocal XRF is a technique that, as XRF tomography, allows obtaining virtual sections of the samples without the need of exposing the inner part (Janssens et al., 2004). For confocal XRF, a polycapillary was used to focus the incoming beam, and a second polycapillary was used between sample and detector (positioned 90° from the incoming beam, and 45° from the sample). In this way, the detected X-rays originate from the small volume created by the intersection between the focused incoming beam and the collimated beam reaching the detector. By moving the sample towards/away from the beam and the detector, the intersection volume is scanned through the sample, allowing the collection of X-ray information from e.g. virtual slices of the sample. The diameter of the focal spot was determined to be approximately 16 μm.

For XRF tomography, mineral grains or particles were scanned over a translation range (x) and a 180° rotation range (ω) with step widths Δx of 15 μm and Δω of 3°, and an acquisition time of 10 s per point. The complete rotational movement (over 180°) occurred clockwise (looking from the top). The conversion of sinograms to tomograms was performed by the statistical maximum-likelihood expectation maximization (MLEM) algorithm (De Nolf and Janssens, 2010).

3. Results and discussion

Digital autoradiography showed a highly heterogeneous distributions of radioactivity at the macroscopic level in soil samples from all three investigated sites (Fig. 1). A large number of the autoradiography-selected samples, and in particular the most active ones or portions of them, was screened by ESEM-EDX.

Bright spots in a backscattered electron image (Fig. 2) indicate areas of high electron density (high Z): this is often a good indication when looking, for instance, for Th hotspots in a lighter matrix. In the most thorium-rich samples, the EDX spectra collected on such hotspots,

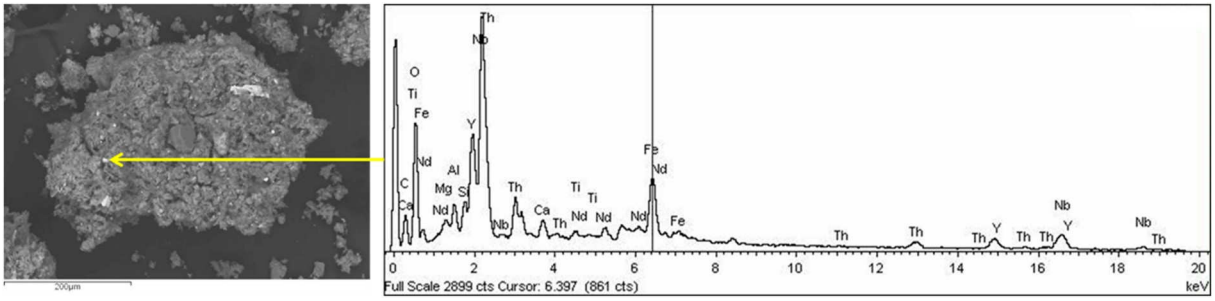

Fig. 2. ESEM-EDX measurement of a sample from Fen-Gruveåsen. The EDX spectrum (right) originates from the bright spot indicated by the arrow in the back-scattered electron image (left).

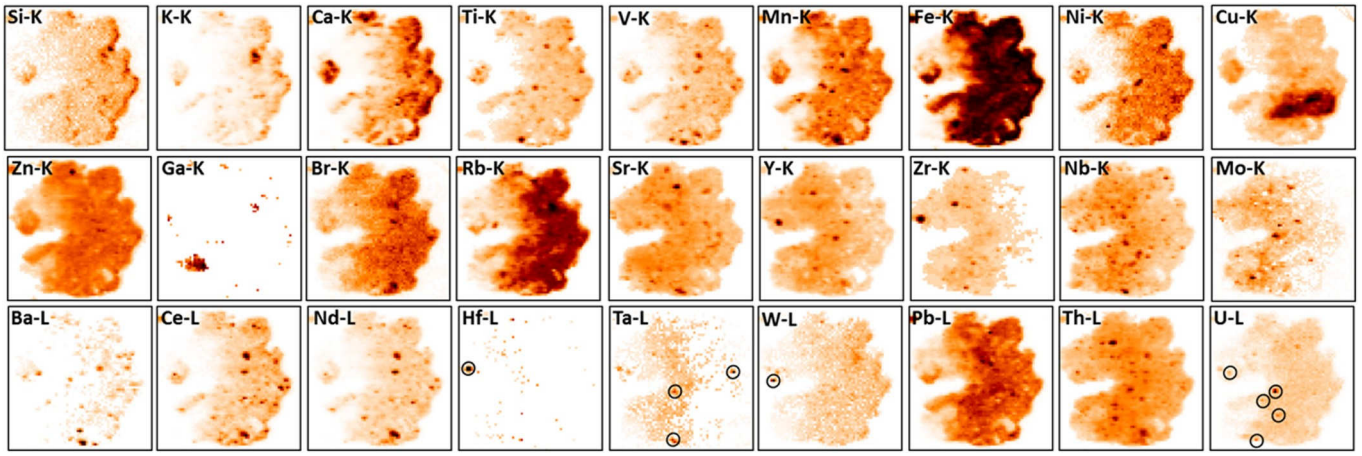

Fig. 3. Elemental μ-XRF maps of a soil particle from the Fen site. For the low-concentration elements Hf, Ta, W and U, their presence is highlighted by black circles around the hotspots where they prevalently occur in their distribution images. Map size: 1950 × 1950 μm^2, step size 30 μm, 7 s/pixel.

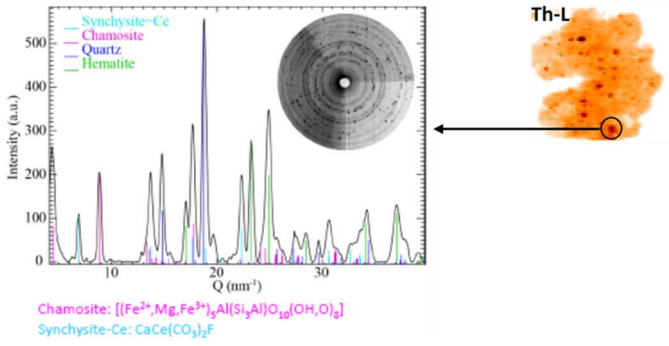

Fig. 4. Results from μ-XRD point measurement in a Th-rich hotspot of a soil particle from the Fen site. The diffractogram (left) was recorded from a hotspot location, indicated by a black circle (right), selected on the basis of the thorium μ-XRF distribution map shown also in Fig. 3.

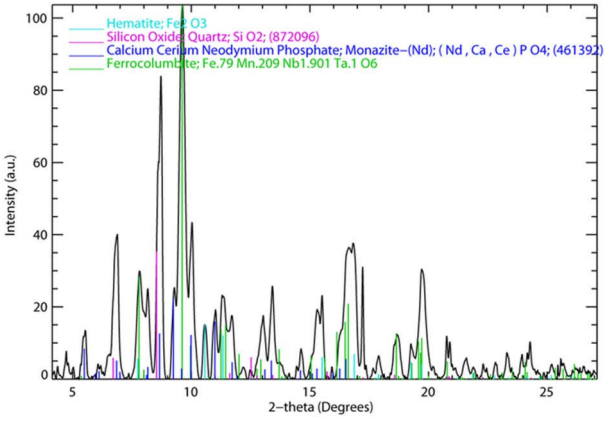

Fig. 5. Results from μ-XRD point measurement in a Th-rich hotspot of a soil particle from the Fen site (elemental distribution maps not shown).

typically show the presence of Th and associated elements such as Y, Nb, next to matrix elements such as Fe and Si.

ESEM-EDX measurements allowed us to directly identify and isolate <1 mm sized Th containing particles and fragments. A selection of these were finally analysed with the set of microscopic techniques (μ-CT, μ-XRF-XRD) described above, in order to image the distribution of actinides and lanthanides with better detection limits and spatial resolution. Indeed, at the HASYLAB beamline L detection limits below 10 ppm can readily be achieved (Falkenberg et al., 2001; Torok et al., 2003). It should be noted that since all these techniques are non-destructive, the samples are preserved for further studies. The results are presented in function of the site of origin of the samples.

3.1. The Fen site

The samples from the Fen site show, next to Th and Y, also Nd and other REE and Nb. Among the low Z elements, next to Si and Fe, Ca, Mg, and P are commonly detected. A selection of μ-XRF and μ-XRD results is shown in Figs. 3–5.

By visually comparing the elemental distribution maps, it emerges that Th is sometimes associated with Nb in hotspots embedded in other minerals. The elemental distributions of the REE Ce and Nd overlap, with occasional co-occurrence in hotspots as well. In a few of these, Th is also present. The improved detection limit compared to ESEM-EDX

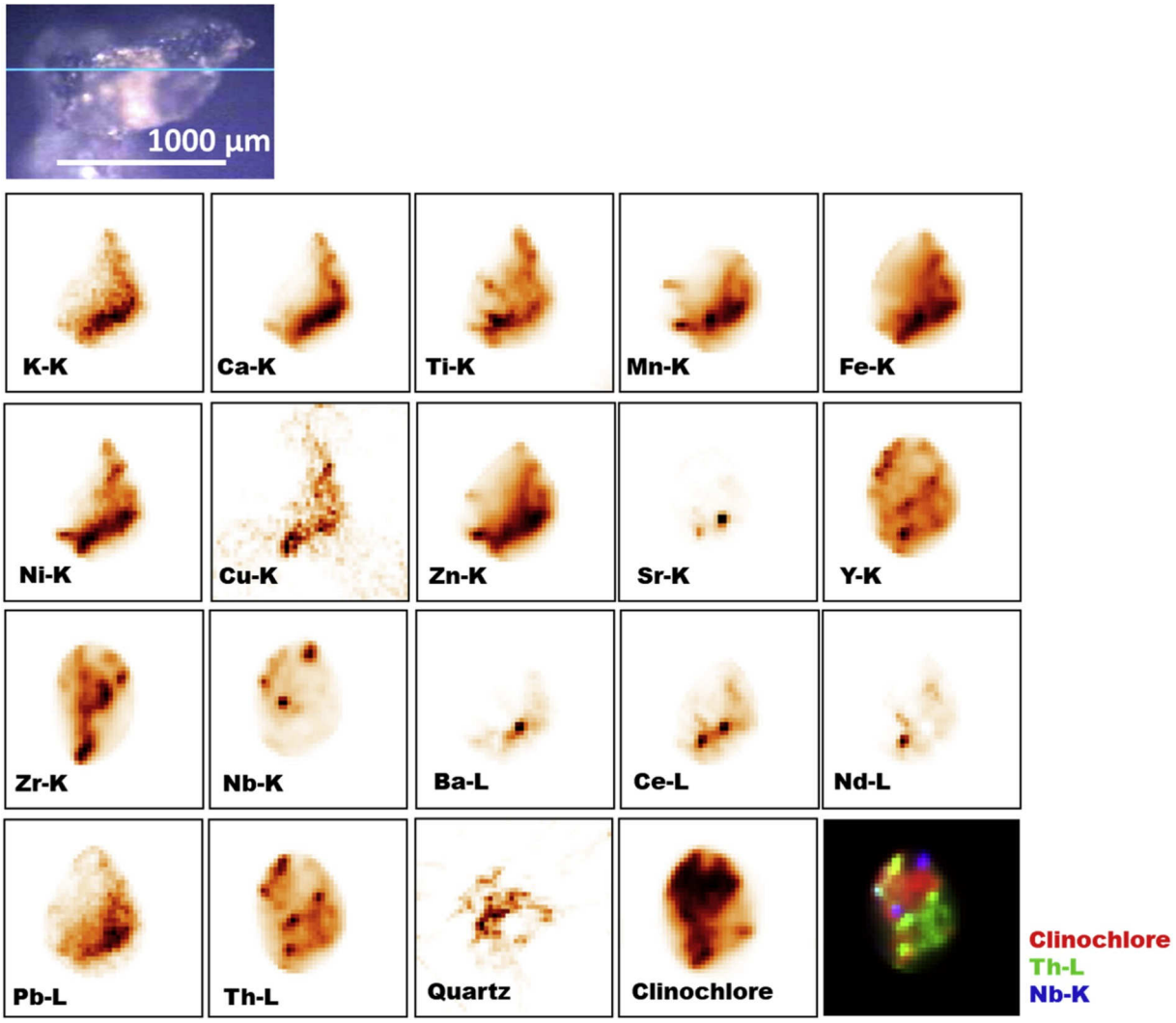

Fig. 6. A Fen-Gruveåsen particle is shown on the top-left, mounted on a capillary as measured with both µ-XRF/XRD tomography and µ-CT. The µ-XRF-XRD tomography results are shown as elemental and mineral distribution maps, collected in a virtual cross section at the position indicated by the horizontal line in the top-left photograph. Map size 2000 × 2000 µm^2, stepsize 20 µm.

allows in some cases to detect U in Th-Nb hotspots (Fig. 3). The typical dimension of such Th-rich grains ranges between 20 and 100 µm. The diffraction patterns show presence of cerium-synchysite [$(CaCe(CO_3)_2F]$ and chamosite [$(Fe^{+2},Fe^{+3},Mg)_5Al(Si_3Al)O_{10}(OH,O)_8$] (Fig. 4). In a different sample from the same site, ferrocolumbite ($FeNb_2O_6$) and possibly neodimium-calcium-cerium-monazite [$Nd,Ca,Ce(PO_4)$] were detected in the Th hotspots (Fig. 5). In both cases, the matrix of the samples at the hotspots is constituted of quartz (SiO_2) and hematite (Fe_2O_3).

In the Fen site, a few samples from the location named Gruveåsen i.e., the former iron mine itself, were analysed. There, the highest Th concentration was expected. An in-depth characterization by XRF, XRD and CT was performed for a specific Gruveåsen sample (Figs. 6–7). There, we find a slightly different element distribution than in other samples of the Fen site.

The XRF-XRD tomography results in Fig. 6 show the distribution of elements and minerals in a virtual slice of this sample. No specific association of Th with other elements is found, besides Y. Pb and Ce rich hotspots are also identified, which are not associated with increased Th levels. A large area on the lower part of the sample, rich in K and Ca, does not show any diffraction signal. Elsewhere in the sample, the only identified minerals are quartz (SiO_2) and clinochlore [$(Mg,Fe^{2+})_5Al(Si_3Al)O_{10}(OH)_8$]. Th-hotspots are located in clinochlore domains.

The µ-CT measurements (Fig. 7) were performed on the entire sample, and not only on a single slice. The results show a spotty aspect in terms of X-ray attenuation. The most attenuating (denser) phase is less abundant and is shown in brighter tones in grayscale, or in red in temperature scale. This denser phase constitutes about 15% of the total volume of the sample. In Fig. 7-F the same slice as in Fig. 6 maps is shown, as retrieved with the CT reconstruction. Based on the identified elements and minerals of Fig. 6, an interpretation of the different features is given, including minerals and Th-hotspots (represented here as striped areas).

By comparing CT and XRF-XRD data, and assuming that the slice shown in Fig. 6 is representative for the whole volume, one can postulate that the entire sample has a rather loose granular structure, with the majority of the grains made of Ca, Fe or Si-rich minerals, and about 15% of the volume made of denser nuggets containing mainly Th.

CT measurements, therefore, could be very useful for the estimation of the potential Th-yields in case industrial separation would be performed. However, this information alone is not enough to support the feasibility of Th recovery, as industrial separation is limited by specific particle size thresholds. Based on the assumption that Th is mainly located in the highest density region, a complete analysis of the CT data stacks was performed, supported by XRF data. This informs us that in the samples of the Fen site most of the Th is rather distributed in low

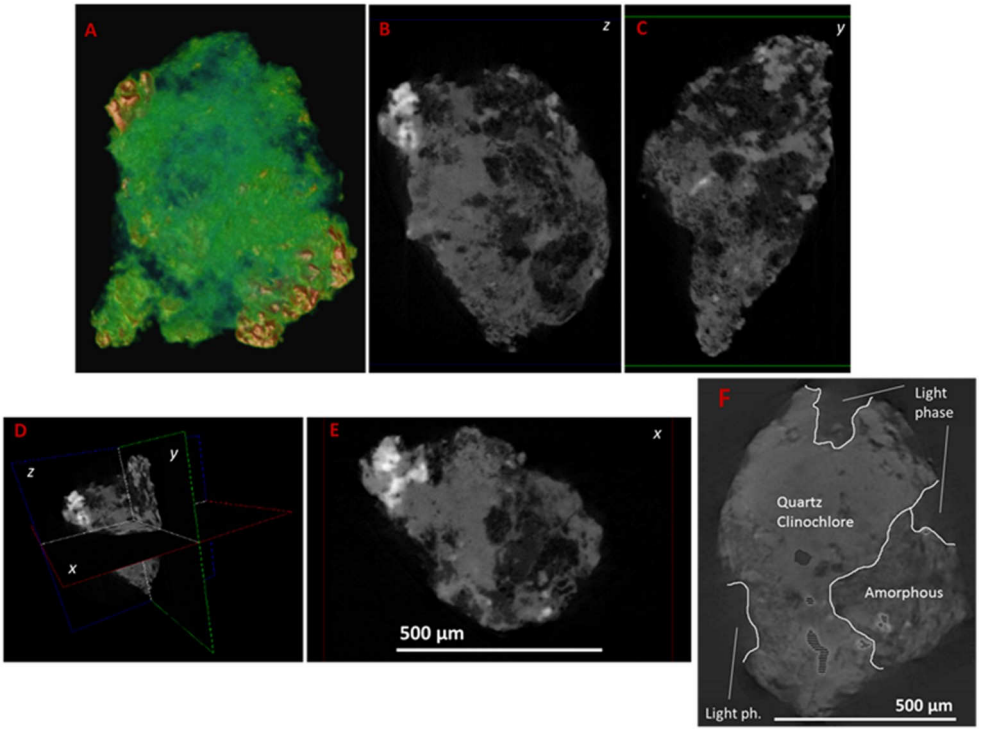

Fig. 7. A–F. µ-CT results of the sample shown in Fig. 6: 3D reconstruction of the whole volume (A) in temperature scale (red = densest, green = lightest); Tomograms on the frontal, median and horizontal plane (B, C, E, respectively) and how they combine (D). Three different phases/materials can be discerned in the tomograms: a denser one (white), a median one (light grey) and the least dense one (dark grey). A µ-CT tomogram (F) was reconstructed with the same position and orientation as the XRF-XRD virtual slice of Fig. 6. Relevant areas are highlighted: thorium hotspots are shown as striped areas. (For interpretation of the references to colour in this figure legend, the reader is referred to the Web version of this article.)

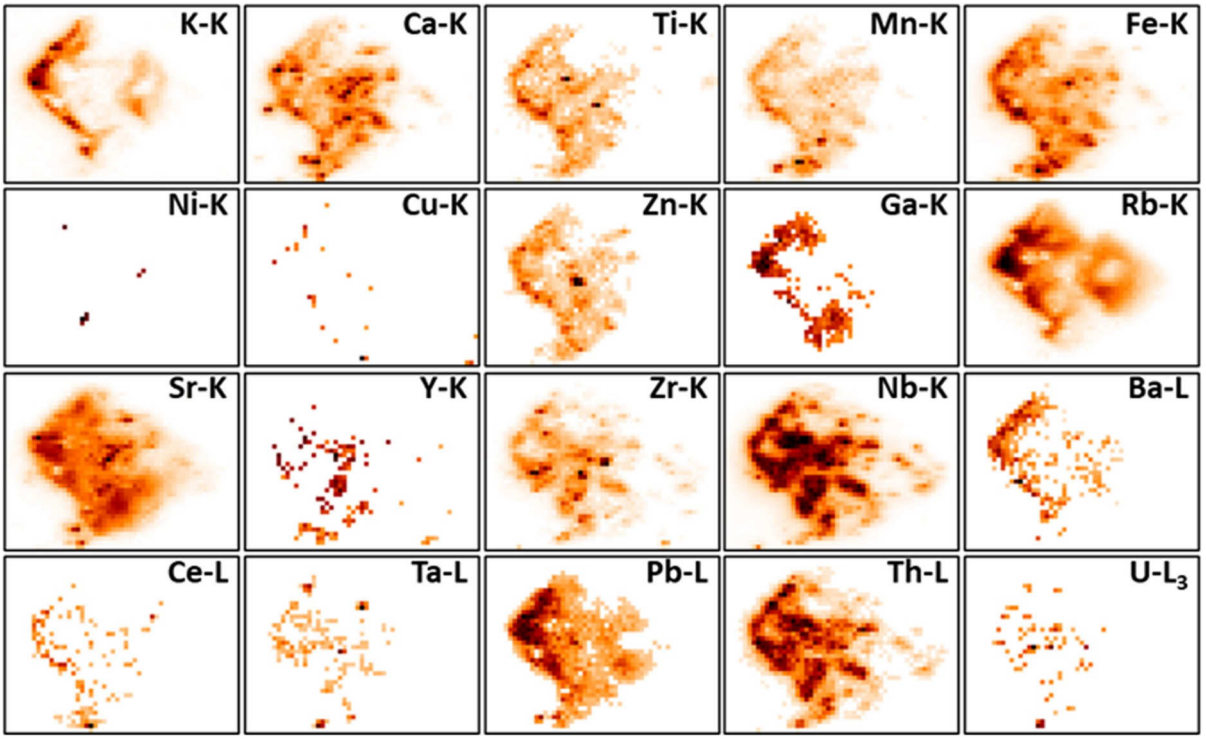

Fig. 8. µ-XRF elemental maps of a soil particle from the Søve site, showing the presence of both Th and U as well as range of metals. Map size 2650 × 2000 µm2, stepsize 50 µm, 1 s per pixel.

quantities and small grains throughout the samples. However, a few larger Th-containing grains occurred, although rarely exceeding a diameter of 100 µm. The Th-ore separation thresholds commonly used in industrial operation are in the range of 20–50 µm (Thorium Report Committee, 2008). Therefore, it is likely that some Th could be effectively recovered for industrial purposes from soil with these characteristics.

3.2. The Søve site

In the samples from the former mining site of Søve, Th is occasionally found to be associated with Pb, besides REE (Fig. 8). In the virtual cross-

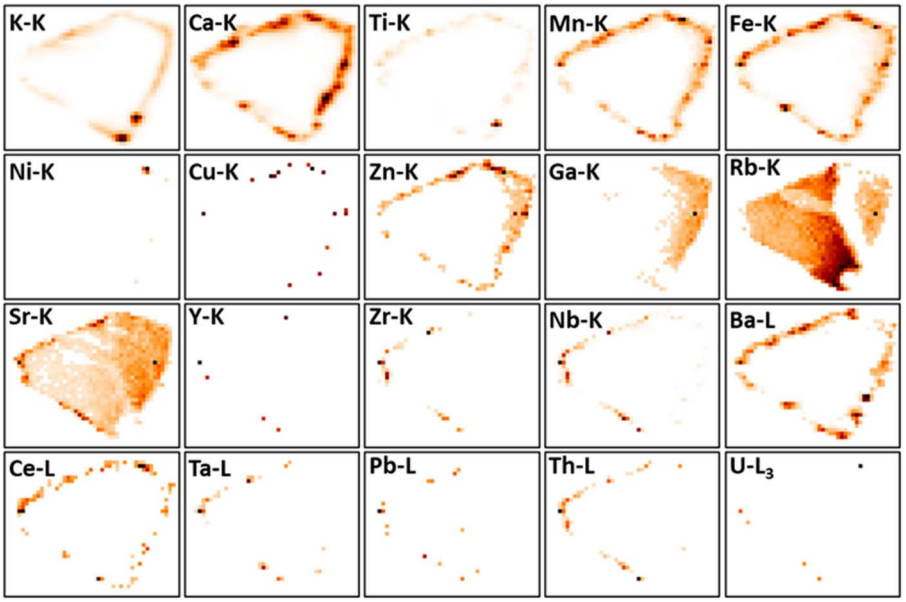

Fig. 9. Confocal μ-XRF virtual cross section of the particle shown in Fig. 8. This figure shows a virtual cross section of the sample, where most elements are visible on the edge only, and only a few show a detectable internal distribution (Rb, Sr). Map size 1150 × 950 μm^2, stepsize 25 μm, 8 s per pixel.

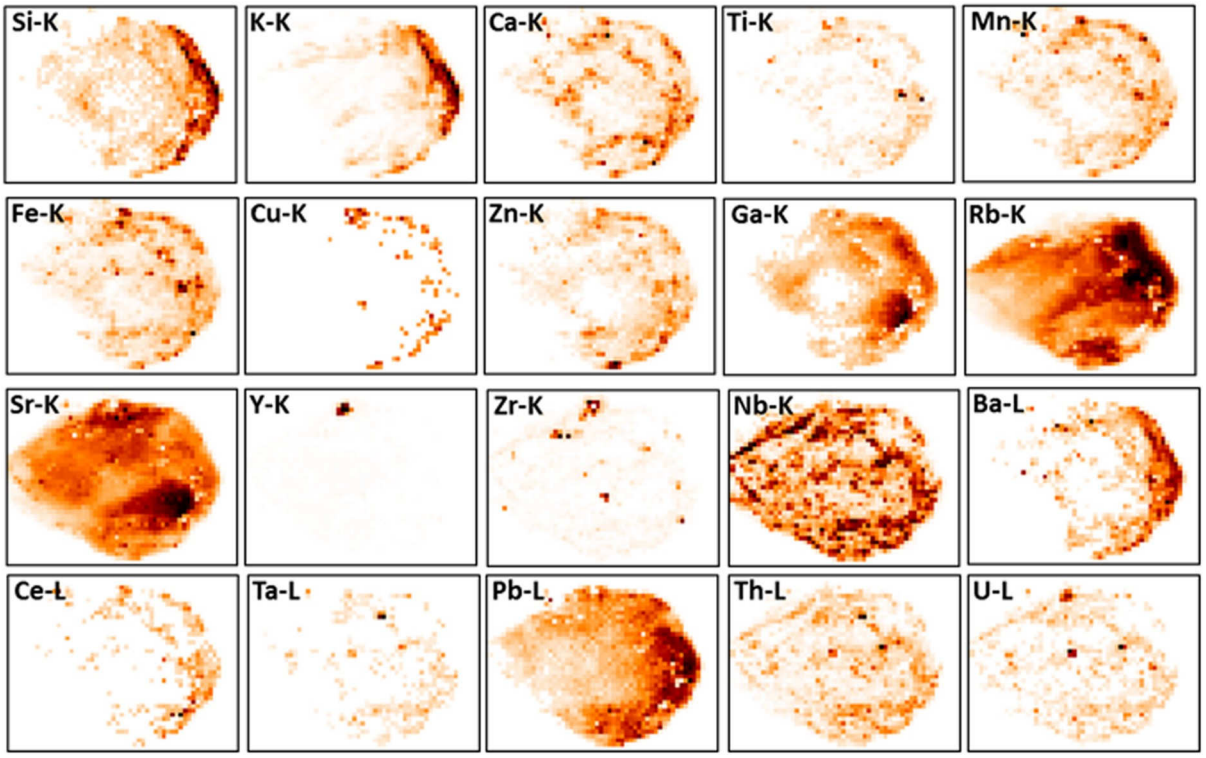

Fig. 10. μ-XRF elemental maps of a soil particle from the Søve site, showing presence of both Th and U. Map size 2650 × 2000 μm^2, stepsize 50 μm, 1 s per pixel.

section of a particle shown in Fig. 9, it is remarkable how the composition of the outer rim (rich in Ca, Mn, Fe, Zn, Ba) is quite different from the inner part, made mostly of Rb and Sr.

In other samples from this area, a similar situation as in the Fen (except Gruveåsen) samples can be seen, with associated abundancy of Nb and Th and hotspots containing Th, and a few points with elevated U concentration (Fig. 10). In most of the Søve samples Sr is observed, typically associated with Ca.

The same sample as in Fig. 8 and 9 was further analysed by means of μ-CT. The results show the existence of three separate phases, a dense one present as hotspots, and two other phases, less dense (Fig. 11). On the basis of a comparison with the XRF data, these three phases can be tentatively identified, in order of increasing X-ray attenuation, as a Rb-rich one, a Sr-rich one and as the Th-containing mineral.

3.3. The Bolladalen site

Selected samples from this undisturbed (i.e. no former mining activities) Th-rich site showed Th XRF signals. In these samples, a similar co-occurrence between Th, REE and Pb was visually observed as in some

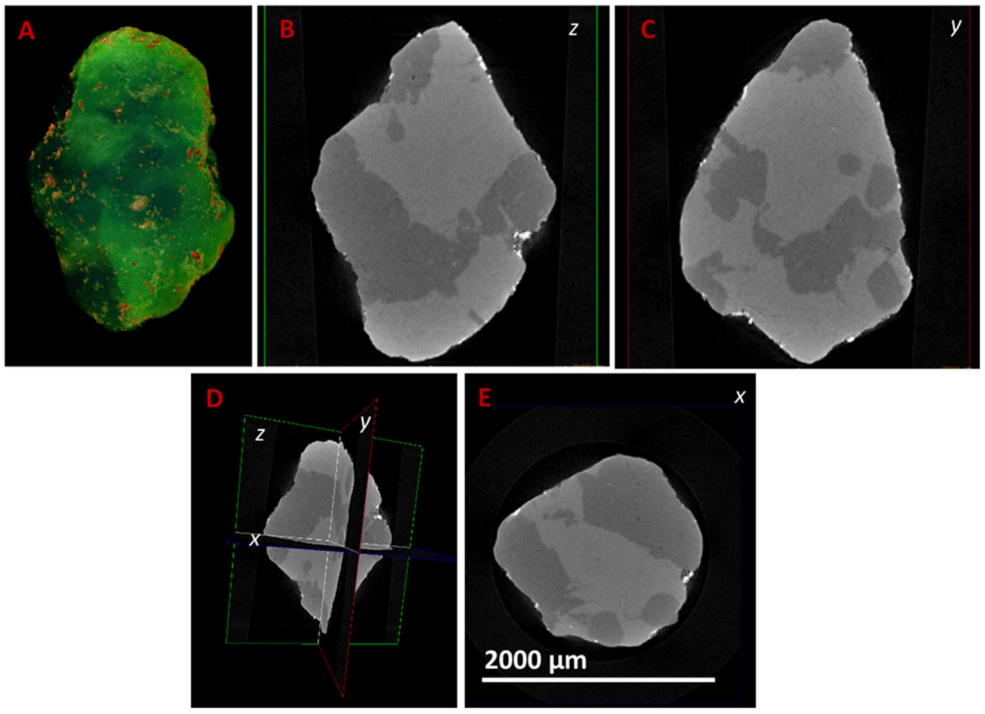

Fig. 11. A–E. µ-CT results of a particle from the Søve site (elemental distribution maps and virtual cross-section shown in Fig. 8 and 9): 3D reconstruction of the whole volume (A) in temperature scale (red = densest, green = lightest); Tomograms on the frontal, median and horizontal plane (B, C, E, respectively) and how they combine (D). Three different phases/materials can be discerned in the tomograms: a denser one (white dots) much less abundant in a matrix made by a median phase (light grey) and a lighter one (dark grey). (For interpretation of the references to colour in this figure legend, the reader is referred to the Web version of this article.)

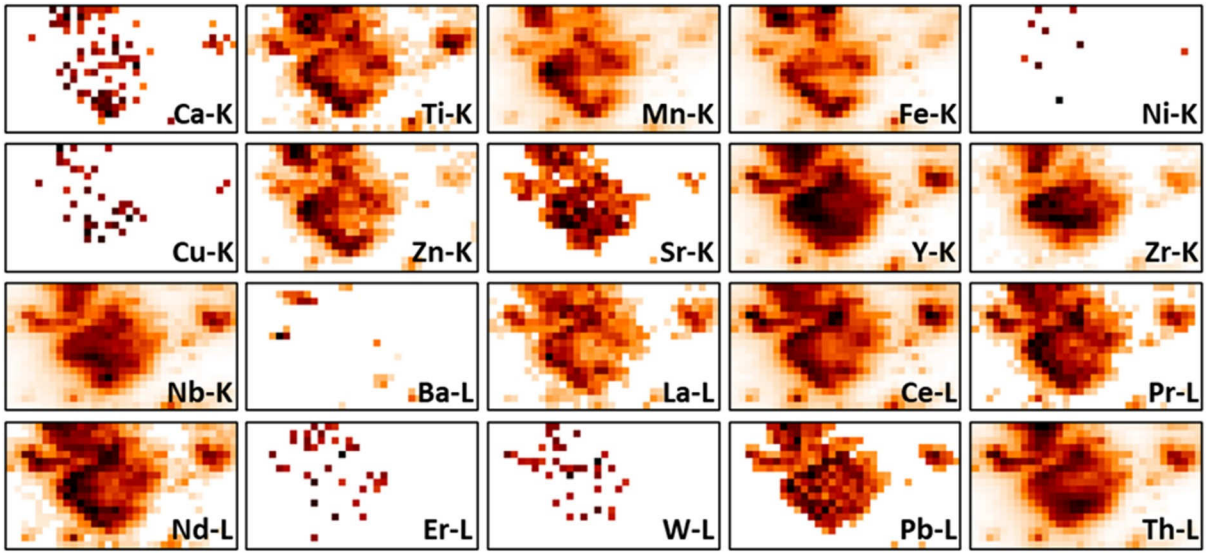

Fig. 12. µ-XRF elemental maps of a soil particle from the Bolladalen site. The XRF lines of La-L, Pr-L and Nd-L are strongly overlapped with Ce-L. Map size: 1650 × 900 µm2, 50 µm step size, 1 s/pixel.

of the Søve samples (Fig. 12) and U and Ra were also detected (Fig. 13).

XRD was performed on Th and U hotspots and diffraction signals were detected that can be assigned to $Sr(U, Th)_{0.5}KNb_5O_{15}$ and $(Ti,Cr)(Ta,Nb)O_4$ (Fig. 14). If the presence of Th in this site was mainly due to the first mineral, it should be verified if the current Th/Ln separation methods, optimized for monazite, a more common Th-containing mineral, would be applicable.

3.4. Radioactive NORM particles in impact and risk assessments

Although previous investigations in the Fen Complex have shown high activity concentrations of NORM in soil of the area, studies on mobilization and uptake of NORM in the Fen biota demonstrated limited bioavailability of NORM. These observations can most probably be attributed to complex environmental conditions governing the solubility of ^{232}Th, ^{238}U and progeny, as well as the abundance of radioactive NORM particles (Mrdakovic Popic et al., 2012, 2014). NORM particles can be re-suspended by erosion, transported atmospherically or in water and lead to potential risks from inhalation and ingestion (Lind et al., 2013).

The uncertainties associated with dispersion and ecosystem transport prediction and dose assessment can be large, if the presence of radioactive hotspots in soils is not adequately considered (Salbu, 2016). In addition, incomplete dissolution of radioactive particles during sample preparation can lead to analytical inconsistencies and irreproducible results (Danesi et al., 2002). Based on the findings in this work,

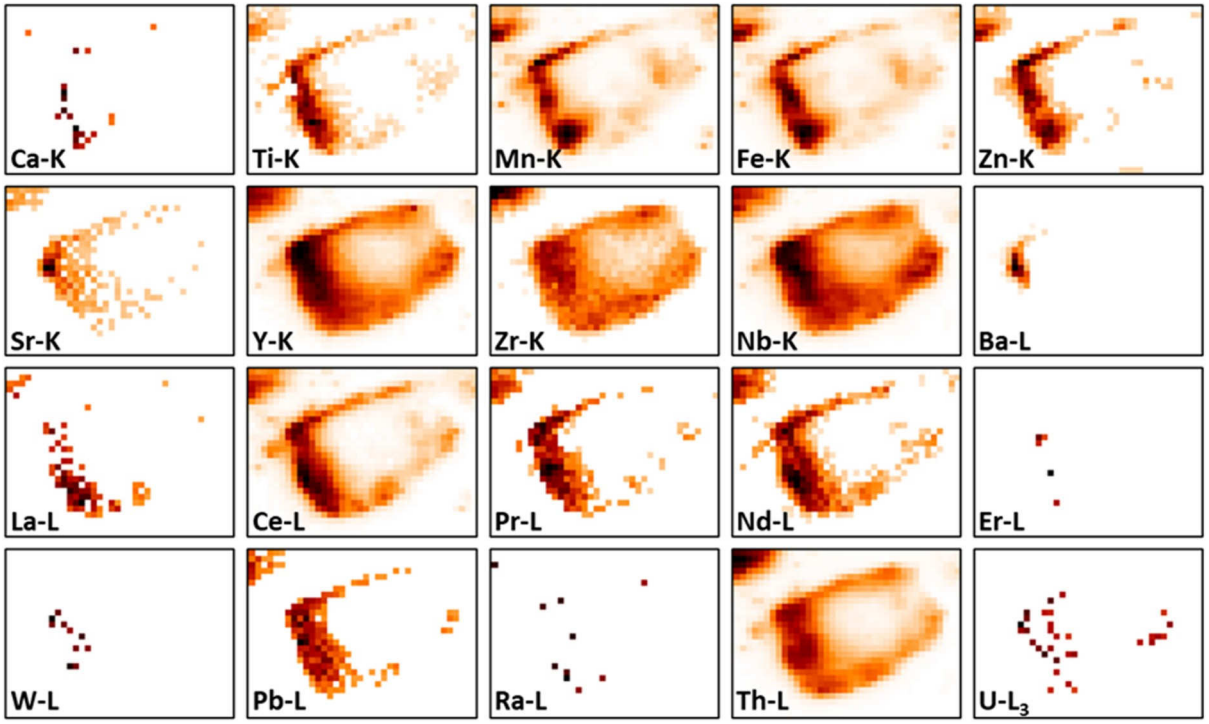

Fig. 13. μ-XRF elemental maps of a soil particle from the Bolladalen site, showing presence of U and Ra. Map size: 1900 × 1400 μm^2 map size, 50 μm step size, 1 s/pixel.

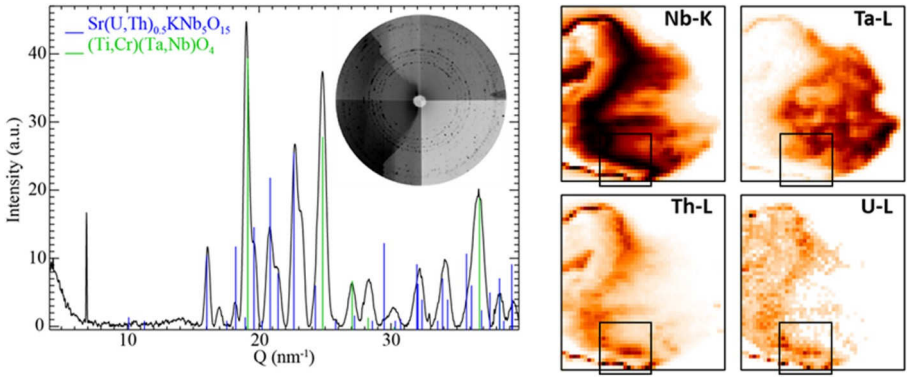

Fig. 14. μ-XRD and μ-XRF analysis of a sample from the Bolladalen site. The XRD diffractogram on the left are recorded in the box marked in the XRF elemental maps on the right, where the higher Th and U intensities are detected.

as well as on previous studies at other NORM sites (Lind et al., 2013), we contend that the presence of heterogeneous distributions including radioactive particles should be anticipated throughout the Fen Complex. Thus, previously obtained results on NORM levels and behaviour in environmental compartments of the Fen Complex should be considered in light of the characterization results presented in the current study. Moreover, screening for radioactive heterogeneities both at the macroscopic and microscopic level, and micro-analytical particle characterization should be implemented when radiological risks are further assessed.

4. Conclusions

In the present work, micro-analytical techniques have been utilised to identify and characterise radioactive particles and fragments containing Th, U and a range of stable metals in soil samples and mineral fragments from the thorium-rich Fen Complex in Norway. In what to the authors' knowledge is the first application of synchrotron micro-beam techniques on Th NORM particles, heterogeneities were characterised on a micrometre(s) scale. The combination of the synchrotron results with those obtained with μ-CT scans of whole particles allowed to extract relevant information on potential thorium occurrence in the investigated areas, in terms of size of Th-containing minerals and relative abundance of those minerals in the analysed volumes. The recent availability of such synchrotron-based techniques with 50 nm resolution or less (Cagno et al., 2017) can open up new avenues for these studies at a higher resolution.

Thorium is found to be mostly present in monazite and Nb-rich minerals, with higher occurrence in the sites of Fen and Søve. In the Fen site, and in particular in the Gruveåsen area, the presence of Th mineral grains with a size around 100 μm might suggest the viability of Th-mining at this site.

The occurrence of Th hotspots at all the investigated sites implies the likely presence of Th-containing particles due to weathering of the Th-rich deposits. Therefore, especially if exploration of ^{232}Th and REE ore should take place, the presence of these particles has to be factored in,

when risk assessment is performed, since this might significantly affect overall environmental behaviour of Th and progeny.

Low mobility and bioavailability of ^{232}Th and high total activity concentrations of ^{232}Th in soil have already been attributed to the occurrence of ^{232}Th in particulate forms. Furthermore, although concentrations of NORM below contamination level have been measured in the water of the nearby lake Nordsjø, measurements of *in-situ* size fractionated water demonstrated presence of about 50% of the total ^{232}Th as particulate matter (high molecular mass species) (Mrdakovic Popic et al., 2014). Based on overall results, the presence of particulate NORM in sediments of the lake, their potential resuspension and transport in the water as well as increased particle transfer in the terrestrial ecosystem and further to biota could not be excluded if environmental conditions change.

Declaration of competing interest

The authors declare that they have no known competing financial interests or personal relationships that could have appeared to influence the work reported in this paper.

Acknowledgements

This project was supported by the Research Council of Norway through its Centres of Excellence funding scheme, project number 223268/F50. Part of this work was also funded by the EC-funded COMET (Contract number: Fission-2012-3.4.1-604794) – RATE (Grant agreement number: 604974) projects. We gratefully acknowledge HASYLAB for granting beamtime. The authors are indebted to Dr. Karen Appel and Dr. Manuela Borchert for beamline assistance.

References

Cagno, S., Brede, D.A., Nuyts, G., Vanmeert, F., Pacureanu, A., Tucoulou, R., Cloetens, P., Falkenberg, G., Janssens, K., Salbu, B., Lind, O.C., 2017. Combined computed nanotomography and nanoscopic x-ray fluorescence imaging of cobalt nanoparticles in caenorhabditis elegans. Anal. Chem. 89 (21), 11435–11442.

Dahlgren, S., 1983. Naturlig Radioaktivitet I Berggrunnen, Gammastrålingskart, Fensfeltet, Telemark, Scale 1:10000 (Prosjekt Temakart, Telemark) (In Norwegian).

Dahlgren, S., 2005. Telemark og Vestfold Rapport 1, 47 (In Norwegian).

Dahlgren, S., 2012. Vestfold fylkeskommuner Rapport 1, 23 (In Norwegian).

Danesi, P.R., Moreno, J., Makarewicz, M., Radecki, Z., 2002. Residual radioactivity in the terrestrial environment of the Muroroa and Fangataufa Atolls nuclear weapon test sites. J. Radioanal. Nucl. Chem. 177, 161–184.

De Nolf, W., Janssens, K., 2010. Micro X-ray diffraction and fluorescence tomography for the study of multilayered automotive paints. Surf. Interface Anal. 42, 411–418.

Falkenberg, G., Clauss, O., Swiderski, A., Tschentscher, T., 2001. Upgrade of the x-ray fluorescence beamline at HASYLAB/DESY. X Ray Spectrom. 30, 170–173.

Falkenberg, G., Rickers, K., Bilderback, D.H., Huang, R., 2004. A Single-Bounce Capillary for Focusing of Hard X-Rays, HASYLAB Annual Report 2003. HASYLAB, Hamburg.

Haquin, G., Yungrais, Z., Ilzycer, D., Zafrir, H., Weisbrod, N., 2017. Detailed effects of particle size and surface area on Rn-222 emanation of a phosphate rock. J. Environ. Radioact. 180, 77–81.

Hoatson, D.M., 2011. The Major Rare Earth Element Deposits of Australia: Geological Setting, Exploration and Resources (Geoscience Australia).

IAEA, 2010. Advanced fuel pellet materials and fuel rod design for water cooled reactors. In: IAEA-TECDOC-1654. IAEA, Vienna.

Janssens, K., Proost, K., Falkenberg, G., 2004. Confocal microscopic X-ray fluorescence at the HASYLAB microfocus beamline: characteristics and possibilities. Spectrochim. Acta B 59, 1637–1645.

Kak, A.C., Slaney, M., 1988. Principles of Computerized TomographicImaging. IEEE Press.

Killeen, P.G., Heier, K.S., 1976. Radioelement distribution and heat production in Precambrian granitic rocks, southern Norway. Acta Polytech. Scand. Phys. 114, 1–31.

Lind, O.C., Stegnar, P., Tolongutov, B.M., Tolongutova, A., Solomatina, A., Rosseland, B. O., Strømman, G., Salbu, B., 2013. Environmental Impact Assessment of radionuclide and metal contamination at the former U site at Kadji-sai, Kyrgyzstan. J. Environ. Radioact. 123, 37–49.

Mrdakovic Popic, J., Salbu, B., Strand, T., Skipperud, L., 2011. Assessment of radionuclides and metals contamination in thorium rich Fen area, Norway. J. Environ. Monit. 13, 1730–1738.

Mrdakovic Popic, J., Salbu, B., Skipperud, L., 2012. Ecological transfer of radionuclides and metals to free-living earthworm species in natural habitats rich in NORM. Sci. Total Environ. 414, 167–176.

Mrdakovic Popic, J., Meland, S., Salbu, B., Skipperud, L., 2014. Mobility of radionuclides and trace elements in soil from legacy NORM and undisturbed naturally 232Th-rich sites. Environ. Sci.: Process Impacts 16 (5), 1124–1134.

NGI-UMB, 2010. Kartlegging Av Omfang Og Kostnader Ved Eventuell Senere Opprydning Av Radioaktivt Materiale Ved Søve Gruver. Norwegian Geotehnical Institute (NGI) and Norwegian University of Life Sciences, Rapport 1927-00-14-R, p. 157 (In Norwegian).

Salbu, B., 2016. Environmental impact and risk assessments and key factors contributing to the overall uncertainties. J. Environ. Radioact. 151 Pt 2, 352–360.

Salbu, B., Lind, O.C., 2020. Analytical techniques for characterizing radioactive particles deposited in the environment. J. Environ. Radioact. 211, 106078 https://doi.org/10.1016/j.jenvrad.2019.106078.

Stranden, E., 1982. En Undersøkelse Av Naturlig Stråling I Fensefeltet Ved Ulefoss. Statens institutt for strålehygiene, SIS - rapport, p. 9 (In Norwegian).

Stranden, E., 1984. Thoron (Rn-220) daughter to radon (Rn-222) daughter ratios in thorium-rich areas. Health Phys. 47 (5), 784–785.

Stranden, E., 1985. The radiological impact of mining in A Th-rich Norwegian area. Health Phys. 48, 415–420.

Sundal, A.V., Strand, T., 2004. Indoor gamma radiation and radon concentrations in a Norwegian carbonatite area. J. Environ. Radioact. 77, 175–189.

Taipale, T.K., 1985. The Samplying and Analyzing Methods of Radionuclides Used in the Nordic Countries for Environmental Samples, Nordic Liaison Committee for Atomic Energy (NKA).

Torok, S., Osan, J., Vincze, L., Alfoldy, B., Kerkapoly, A., Vajda, N., Perez, C.A., Falkenberg, G., 2003. Comparison of nuclear and X-ray techniques for actinide analysis of environmental hot particles. J. Anal. Atomic Spectrom. 18, 1202–1209.

Thorium Report Committee, 2008. In: Thorium as an Energy Source - Opportunities for Norway. Ed: Research Council of Norway (RCN), on Behalf of the Ministry of Petroleum and Energy (OED), ISBN 978-82-7017-692-2 (printed) ISBN 978-82-7017-693-9 (electronic).

US EPA, 2014. Soil Sampling Protocole, SESDPROC-300-R3, R3.